UV and Photoelectron Spectrum of Carbonyl Fluoride, F_2CO. Multireference Configuration Interaction Studies in C_{2v} Symmetry

Friedrich Grein

Department of Chemistry, University of New Brunswick, Fredericton, NB E3B 6E2, Canada

Received: July 29, 1998; In Final Form: October 19, 1998

Using multireference CI methods for F_2CO in C_{2v} symmetry, with near triple-ζ basis sets and added polarization and diffuse functions, CO, CF, and FCF potentials were calculated for four states each of $^1A_1$, $^1B_1$, $^1B_2$, and $^1A_2$ symmetry. Vertical excitation energies were obtained for six roots, both for singlet and triplet states. Also, vertical and some adiabatic ionization potentials of F_2CO were calculated. System I of the UV absorption spectrum is clearly $n_o \rightarrow \pi^*$. System II, ranging from 7.02 to 7.66 eV, can only be assigned to triplet $\pi \rightarrow \pi^*$. System III is most likely $n_o \rightarrow 3s/n_o \rightarrow \sigma^*$. System IV, a continuum, is assigned to $\pi \rightarrow \pi^*$, on the basis of its large oscillator strength. Following calculated ionization potentials (IP), the 17.2 eV photoelectron band is assigned to $8a_1$ and the 16.6 eV one to $4b_2$. This way, up to the eighth IP, calculated and experimental values agree within 0.2 eV. The perfluoro effect has been reinvestigated. Calculated vibrational frequencies of the three lowest states of F_2CO^+ are used for an understanding of the vibrational structure of the photoelectron spectrum.

Introduction

In recent studies by this group, the UV and photoelectron spectra of H_2CO[1−6] and Cl_2CO[7] were investigated theoretically. It has been shown how the $^1(\pi,\pi^*)$ state of H_2CO, not seen directly, transfers its intensity to various Rydberg states. The potential curve of $^1(\pi\pi^*)$, calculated as a function of the CO distance, crosses all n- and π-series Rydberg states. On the other hand, for Cl_2CO the CO potential curve of $^1(\pi\pi^*)$ lies well below the Rydberg potentials, as confirmed by the observed B ← X system corresponding to the $\pi \rightarrow \pi^*$ transition.

For carbonyl fluoride, F_2CO, experimental investigations up to 1978[8−13] are cited in the paper by Vasudevan and Grein.[14] Most significant is the work by Workman and Duncan,[9] which was summarized by Robin.[15]

Accordingly, the observed system I ranges from 5.22 to about 6.95 eV. It has a low oscillator strength of $f = 3 \times 10^{-4}$ and a complex vibrational structure and is assigned to $n \rightarrow \pi^*$. System II, from 7.02 to 7.66 eV, has a structure similar to that of system I, with a maximum at 7.34 eV and $f = 5 \times 10^{-4}$. Transitions $n \rightarrow \pi^{*\prime}$, a second π^* orbital resulting from the $2p_x$ AO's on F, and $n \rightarrow \sigma^*$ and $\pi \rightarrow \sigma^*$ have been suggested. System III, from 8.13 to 8.52 eV with $f = 1 \times 10^{-3}$ and a maximum at 8.42 eV, shows a progression of five bands. Around 8.5 eV, a continuous absorption starts (system IV), which has a maximum at 9.42 eV and $f = 0.15$. System III has tentatively been assigned to $n \rightarrow \sigma^*$ or $n \rightarrow 3s$, and system IV to $\pi \rightarrow \pi^*$ or $n \rightarrow 3s$. A summary of the observed electronic spectrum of F_2CO appears in Table 1.

More recently, Judge and Moule[16] reanalyzed system I. The origin was placed at 4.86 eV. The excited state labeled system I is found to be nonplanar, as in H_2CO, with an out-of-plane angle of 31.8° and a barrier to planarity of 1.02 eV. The observed 170 bands were assigned to the frequencies $\nu_1'-\nu_5'$.

In 1978, Vasudevan and Grein[14] presented vertical excitation energies for low-lying singlet and triplet states of F_2CO, calculated by multireference (MR) configuration interaction (CI) methods. They confirmed system I to be $^1(n \rightarrow \pi^*)$, but found no singlet state in the energy region of system II. Instead, a triplet $\pi \rightarrow \pi^*$ excitation was assigned. For systems III and IV, $^1(n \rightarrow 3s)$ and $^1(\pi \rightarrow \pi^*)$, respectively, could be confirmed. Brewer and Schug in 1980[17] calculated CO potential curves for the lowest singlet and triplet states by the PUHF method and looked at the photodissociation $F_2CO \rightarrow CF_2 + O$. Kapur et al.[18] calculated out-of-plane bending potentials for several carbonyl compounds. For the $^3(n\pi^*)$ state of F_2CO, an out-of-plane angle of 49.1° and a barrier of 0.72 eV was obtained. Compared to other carbonyl compounds XYCO, with X,Y = H, F, Cl, F_2CO has the largest out-of-plane angle and the highest barrier.

Geometry optimizations on the ground state (GS) of F_2CO, as well as the lowest $^{1,3}A_2$, $^{1,3}A''(n\pi^*)$, and $^3A'(\pi\pi^*)$ states, were carried out by Francisco et al.[19] using UMP2, QCISD, and CASSCF methods with 6-31G*, 6-311G*, and 6-311+G-(2d) basis sets. Also, harmonic frequencies were obtained for the GS as well as the $^{1,3}A_2$ and $^1A''$ states. The adiabatic excitation energy T_e of nonplanar $^1(n\pi^*)$ is 4.23−4.82 eV, depending on the method. Including zero-point energies, the CASSCF estimate for T_o is 4.76 eV, close to the value given by Judge and Moule.[16]

Francisco et al.[20−22] studied decomposition reactions of larger molecules that include F_2CO among the products. Sumathi and Chandra[23] investigated the decomposition of F_2CO on its lowest triplet surface.

In the present paper, MRCI potential energy curves involving CO and CF displacements, as well as changes of the FCF angle, will be given. Also, the lower ionization potentials have been obtained. On the basis of these results, the observed UV and photoelectron spectra of carbonyl fluoride are to be investigated.

It is realized that for a polyatomic molecule like carbonyl fluoride, potential energy curves only contain limited information on the structure and properties of excited states and that extensive potential surfaces are needed to better understand the spectra. Nevertheless, from the results presented here, some

10.1021/jp983215s CCC: $15.00
Published on Web 12/05/1998

TABLE 1: Observed Electronic Spectrum of F_2CO[a]

system	range (eV)	ΔE (max)	oscillator strength	vib bands	tentative assignt	VG assignt
I	4.86[b] to ~6.95		3×10^{-4}	170[b]	$n \rightarrow \pi^*$	$^1(n \rightarrow \pi^*)$
II	7.02−7.66	7.34	5×10^{-4}	20	$n \rightarrow \pi^{*\prime}$, $n \rightarrow \sigma^*$, $\pi \rightarrow \sigma^*$	$^3(\pi \rightarrow \pi)^*$
III	8.13−8.52	8.42	1×10^{-3}	5	$n \rightarrow \sigma^*$, $n \rightarrow 3s$	$^1(n \rightarrow 3s)$
IV	~8.5−	9.42	0.15	cont	$\pi \rightarrow \pi^*$, $n \rightarrow 3s$	$^1(\pi \rightarrow \pi^*)$

[a] Experimental values from ref 9, unless otherwise indicated. VG: Vasudevan and Grein, ref 14, theoretical work. [b] Reference 16.

useful conclusions about the interpretation of observed spectra can be drawn.

Methods and Molecular Orbitals

For all calculations on excited states, the multireference single and double excitation method "MRD-CI"[24−28] was used in the recent direct-CI implementation by Pless, Suter, and Engels.[29] All configurations having $c^2 \geq M$ (main selection threshold, usually 0.002) were included in the set of reference configurations (from about 30 to 70). Out of 5−20 million generated symmetry-adapted functions, about 200 000 were selected for diagonalization of the secular equations. The configuration selection threshold T is usually 1 or 2 μhartree. Four to six roots were calculated. In all cases, the core orbitals (1s of each atom) were frozen, and the complementary highest MO's discarded. Either extrapolated, or weighted extrapolated energies with Davidson correction, will be given.

Basis set A uses the Huzinaga−Dunning 10s6p/5s3p contraction for C and F and the 12s8p/5s4p contraction for O.[30] For each atom, one d-polarization function (C, 0.75; F, 0.90; O, 0.85) was added, and for C three Rydberg functions (s, 0.023; p, 0.021; d, 0.015) were added. In conjunction with basis set A having 93 contracted functions, $^3(n\pi^*)$ MO's were used.

Basis set B consists of the 10s6p/5s3p contraction plus one polarization function for each atom, and additional s,p,d Rydberg functions on C (as above). On O and F, p-negative ion functions were placed.[31] With 99 contracted functions in basis B, ground-state MO's are used in the CI wave function.

For all calculations presented in this paper, F_2CO is kept planar, lying in the yz plane and having C_{2v} symmetry. For the ground-state geometry, microwave values from Carpenter,[32] with $R_{CO} = 1.1700$ Å (2.2110 a_0), $R_{CF} = 1.3166$ Å (2.4880 a_0), and $\phi(FCF) = 107.6°$, were chosen. They are very similar to microwave results from Nakata et al.[33]

At equilibrium geometry, the GS configuration is $(1-8)a_1^2(1-2)b_1^2(1-5)b_2^2 1a_2^2$. Occupied MO's playing a significant role in the CI wave functions are $6a_1 = \sigma'$, $7a_1 = n_{a1}(F)$, $8a_1 = \sigma$, $1b_1 = n_{b1}(F)$, $2b_1 = \pi$, $4b_2 = n_{b2}(F)$, $5b_2 = n_o$, and $1a_2 = n_{a2}(F)$, where the MO's labeled n(F) are essentially fluorine lone-pair MO's. In basis set A, n_o lies well above $n_{b2}(F)$ owing to optimization for $n\pi^*$ MO's. In basis set B, however, n_o also has some F lone-pair character.

Important virtual orbitals are $(9-12)a_1$, which are the Rydberg MO's 3s, $3p_z$, $3d_{z^2}$, and $3d_{x^2-y^2}$, $14a_1 = \sigma^*$, $3b_1 = 3p_x$, $4b_1 = 3d_{xz}$, $5b_1 = \pi^*$, $6b_2 = 3p_y$, $7b_2 = 3d_{yz}$, $8b_2 = \sigma_{b2}^*$, and $2a_2 = 3d_{xy}$. The Rydberg MO's do not separate well into s, p, and d components within the same symmetry species. The designation of Rydberg states is based mainly on the ordering of states in the CI results. At larger CO and CF distances, the orbital character is changing, as will be outlined in the appropriate sections.

In Table 2, orbital energies and notations will be given for the MO's HOMO − 1 to LUMO + 1 or LUMO + 2, using basis B, at the experimental GS geometry. For later comparison, corresponding orbital energies for H_2CO and Cl_2CO, obtained from similar basis sets, are included.

TABLE 2: Orbital Energies ϵ and MO Notation for F_2CO, Cl_2CO, and H_2CO at Respective Ground-State Equilibrium Geometry

		F_2CO		Cl_2CO		H_2CO	
MO[a]		ϵ (au)	not.[b]	ϵ (au)	not.[b]	ϵ (au)	not.[b]
				a_1 MO's			
HO-1	($7a_1$)	−0.806	n_{a1}	−0.706	σ'	−0.871	σ'
HO	($8a_1$)	−0.707	σ	−0.532	σ	−0.654	σ
LU	($9a_1$)	0.016	3s	0.018	3s	0.002	3s
LU+1	($10a_1$)	0.049	$3p_z$	0.050	$3p_z$	0.010	$3p_z$
				b_1 MO's			
HO-1	($1b_1$)	−0.819	n_{b1}	−0.653	π	−0.538	π
HO	($2b_1$)	−0.579	π	−0.499	n_{b1}	0.010	$3p_x$
LU	($3b_1$)	0.045	$3p_x$	0.051	$3p_x$	0.013	$3d_{xz}$
LU+1	($4b_1$)	0.050	$3d_{xz}$	0.054	$3d_{xz}$	0.129	π^*
LU+2	($5b_1$)	0.152	π^*	0.104	π^*		
				b_2 MO's			
HO-1	($4b_2$)	−0.705	n_{b2}	−0.497	n_{b2}	−0.696	σ_{CH_2}
HO	($5b_2$)	−0.561	n_o	−0.477	n_o	−0.433	n_o
LU	($6b_2$)	0.049	$3p_y$	0.054	$3p_y$	0.010	$3p_y$
LU+1	($7b_2$)	0.052	$3d_{yz}$	0.062	$3d_{yz}$	0.013	$3d_{yz}$
				a_2 MO's			
HO	($1a_2$)	−0.728	n_{a2}	−0.502	n_{a2}		
LU	($2a_2$)	0.051	$3d_{xy}$	0.054	$3d_{xy}$	0.011	$3d_{xy}$

[a] The MO number given corresponds to F_2CO. [b] Notation of MO.

For the GS and $^3(\pi\pi^*)$ states of F_2CO and for lower states of F_2CO^+, Gaussian 90[34] geometry optimizations and frequency calculations were performed.

Results

(1) Optimized Geometries and Frequencies for F_2CO and F_2CO^+. In Table 3, optimized geometries and harmonic frequencies are given, as obtained from Gaussian 90 calculations using the MP2/UMP2 method with a 6-311G* basis set, for the GS of F_2CO, as well as the X^2B_2 ($n_o \rightarrow \infty$), 1^2B_1 ($\pi \rightarrow \infty$), and 1^2A_1 ($\sigma \rightarrow \infty$) states of F_2CO^+.

For the GS of F_2CO, both optimized geometry and vibrational frequencies are in good to excellent agreement with experimental numbers,[32,33,35] as has also been found by others.[19,36]

For the GS of F_2CO^+ ($n_o \rightarrow \infty$), R_{CO} increases and R_{CF} decreases, indicating that n_o is CO bonding and CF antibonding. Removal of a π-electron from F_2CO in its ground state, leading to the 1^2B_1 state of F_2CO^+, results in a lengthening of the CO bond by 0.14 Å (0.27 a_0) and a shortening of the CF bond by 0.08 Å (0.15 a_0), the latter amount being almost the same as for X^2B_2. The 1^2A_1 ($\sigma \rightarrow \infty$) state has similar geometries and frequencies as X^2B_2, so the σ MO (really n_{a1}) is not unlike n_o. For all ionic states, the FCF angle increases by about 10°.

The changes in the stretching frequencies of X^2B_2, relative to the GS of F_2CO, reflect the changes in bond distances. A significant increase in frequency is noticed for the asymmetric CF_2 stretch.

Adiabatic ionization potentials (IP) of F_2CO, calculated from the energies given in Table 3, are 12.79 eV for $n_o \rightarrow \infty$, 13.93 eV for $\pi \rightarrow \infty$, and 16.99 eV for $\sigma \rightarrow \infty$. Corresponding experimental values are 13.02, 14.09, and 16.1 eV,[36] showing

TABLE 3: MP2/6-311G* Optimized Geometries (Distances in Å), Harmonic Frequencies (in cm^{-1}), and Energies (in au) for the Ground State of F_2CO, as Well as the X^2B_2, 1^2B_1, and 1^2A_1 States of F_2CO^+ [a]

		F_2CO (X^1A_1)	F_2CO^+ (X^2B_2)	F_2CO^+ (1^2B_1)	F_2CO^+ (1^2A_1)
R_{CO}		1.1760 (1.1700)[b]	1.2697	1.3168	1.2610
R_{CF}		1.3173 (1.3166)[b]	1.2405	1.2346	1.2416
ϕ(FCF)		107.55 (107.6)[b]	120.88	118.18	120.26
E_{MP2}/E_{UMP2}		−312.4288	−311.9588	−311.9169	−311.8043
CF_2-sb	(a_1)	591.4 (584)[c]	579.0 (530)[d]	613.9	603.3
CF_2-ab	(b_2)	627.6 (626)[c]	499.0	557.2	655.3
OOP	(b_1)	789.9 (774)[c]	788.4	743.7	828.9
CF_2-ss	(a_1)	978.2 (965)[c]	1059.6	1023.9	1070.9
CF_2-as	(b_2)	1268.8 (1249)[c]	1654.5	1681.1	1623.3
CO-ss	(a_1)	2000.5 (1942)[c]	1694.6 (1550)[d]	1569.6	1624.1

[a] Experimental values in parentheses. Calculated vibrational intensities, in km/m, are the following, in order of vibrational listing: for X^1A_1, 7.0, 8.0, 37.7, 64.8, 453.1, 427.9; for X^2B_2, 14.9, 18.6, 52.1, 7.3, 456.3, 316.0. [b] Reference 32. [c] Reference 35. [d] Reference 37.

TABLE 4: Vertical Excitation Energies ΔE and Oscillator Strengths f for Singlet States of F_2CO, Using Basis Set B

state	ΔE (eV)	config	f	state	ΔE (eV)	config	f
1^1A_1	0.00	GS		1^1B_2	9.47	n_o3s	0.039
2^1A_1	10.18	$\pi\pi^*$	0.254	2^1B_2	11.20	n_o3p_z	0.000
3^1A_1	11.25	n_o3p_y	0.074	3^1B_2	11.82	$n_o3d_{z^2}$	0.002
4^1A_1	11.98	n_o3d_{yz}	0.001	4^1B_2	11.88	n_o3d_{x2-y2}	0.006
5^1A_1	12.19	$\pi3p_x$		5^1B_2	13.96	$n_o\sigma^*$	
6^1A_1	13.25	$\pi3d_{xz}$					
1^1B_1	10.67	$\pi3s$	0.017	1^1A_2	7.35	$n_o\pi^*$	0
2^1B_1	11.31	$\sigma\pi^*$	0.020	2^1A_2	10.86	n_o3p_x	0
3^1B_1	12.41	$\pi3p_z$	0.002	3^1A_2	11.72	$n_{b2}\pi^*$	0
4^1B_1	12.84	$\pi3d_{z^2}$	0.007	4^1A_2	11.94	n_o3d_{xz}	0
5^1B_1	13.26	$\pi3d_{x^2-y^2}$		5^1A_2	13.90	$n_o\pi^{*\prime}$	0

good agreement for the first two IP's. The apparent lesser agreement for $\sigma \rightarrow \infty$ will be discussed later.

(2) Vertical Excitation Energies for F_2CO. Vertical excitation energies were calculated for the six lowest states, using basis set B. Weighted extrapolated energies including the Davidson correction are given.

The results for singlet states are shown in Table 4. Except for $^1A_1$ states, only five roots are given, since the sixth root corresponds to a high valence state but should be a 4s or 4p Rydberg state for which the basis set is insufficient. Also, the leading configurations and oscillator strengths, calculated from wave functions with a higher threshold T of 20 μhartree, are given.

With regard to the $^1A_1$ states, the GS is followed by $\pi\pi^*$, n_o3p_y, n_o3d_{yz}, $\pi3p_x$, and $\pi3d_{xz}$. For the $^1B_1$ states, the ordering is $\pi3s$, $\sigma\pi^*$, $\pi3p_z$, $\pi3d_{z^2}$ and $\pi3d_{x^2-y^2}$. For $^1B_2$, the four Rydberg states n_o3s, n_o3p_z, $n_o3d_{z^2}$, $n_o3d_{x^2-y^2}$ are followed by $n_o\sigma^*$. For $^1A_2$, as expected, $n_o\pi^*$ is the lowest followed by n_o3p_x, $n_{b2}\pi^*$, n_o3d_{xz}, and $n_o\pi^{*\prime}$. At energies lower than the valence states 5^1B_2 and 5^1A_2, $n = 4$ Rydberg states are expected.

The $\pi\pi^*$ state has the highest oscillator strength, 0.25, followed by n_o3p_y (0.07), n_o3s (0.04), and $\sigma\pi^*$ (0.02). Both n_o3p_y and n_o3s mix heavily, at the GS geometry, with the valence states $\pi\pi^*$ and $n_o\sigma^*$, respectively, as the potential curves will show. This leads to intensity transfer from valence to Rydberg states.

Vertical excitation energies of triplet states are given in Table 5. In almost all cases, the ordering of the triplet states is the same as that of singlet states.

A comparison of ΔE values for corresponding singlet and triplet states, divided into categories such as π^* valence states, is shown in Table 6. One sees that triplet π^* valence-state energies are 0.35−1 eV lower than their singlet counterparts, with the exception of $\pi\pi^*$, whose triplet energy is lowered by 2.8 eV. For the only σ^* valence state listed, the energies are about the same. For Rydberg states, the triplet energies are virtually the same as the singlet energies, except for the lowest ones, n_o3s and $\pi3s$, being 0.3−0.4 eV lower in the triplet case. Please note that the state numbering for singlet and triplet states having the same configuration is not necessarily the same. For example, the $n_{b2}\pi^*$ configuration is present in 3^1A_2 and 4^3A_2.

TABLE 5: Vertical Excitation Energies ΔE for Triplet States of F_2CO, Using Basis Set B

state	ΔE (eV)	config	state	ΔE (eV)	config
1^3A_1	7.36	$\pi\pi^*$	1^3B_2	9.12	n_o3s
2^3A_1	11.05	n_o3p_y	2^3B_2	11.01	n_o3p_z
3^3A_1	11.88	n_o3d_{yz}	3^3B_2	11.80	$n_o3d_{z^2}$
4^3A_1	11.98	$\pi3p_x$	4^3B_2	11.82	$n_o3d_{x^2-y^2}$
5^3A_1	12.75	$n_o\sigma^*_{b2}$	5^3B_2	11.94	n_o4s
6^3A_1	13.19	$\pi3d_{xz}$			
1^3B_1	10.20	$\pi3s$	1^3A_2	7.01	$n_o\pi^*$
2^3B_1	10.36	$\sigma\pi^*$	2^3A_2	10.90	n_o3p_x
3^3B_1	12.42	$\pi3p_z$	3^3A_2	10.97	n_o3d_{xz}
4^3B_1	12.75	$\pi3d_{z^2}$	4^3A_2	11.71	$n_{b2}\pi^*$
5^3B_1	13.15	$\pi3d_{x^2-y^2}$	5^3A_2	13.84	$n_o\pi^{*\prime}$

TABLE 6: Comparison of Vertical Excitation Energies ΔE (in eV) for Singlet and Triplet States of F_2CO

	singlet		triplet	
configuration	state	ΔE	state	ΔE
	π^* Valence States			
$n_o\pi^*$	1^1A_2	7.35	1^3A_2	7.01
$\pi\pi^*$	2^1A_1	10.18	1^3A_1	7.36
$\sigma\pi^*$	2^1B_1	11.31	2^3B_1	10.36
$n_{b2}\pi^*$	3^1A_2	11.72	4^3A_2	10.71
	σ^* Valence States			
$n_o\sigma^*$	5^1B_2	13.96	6^3B_2	13.82
	n_o Rydberg States			
n_o3s	1^1B_2	9.47	1^3B_2	9.12
n_o3p_x	2^1A_2	10.86	2^3A_2	10.90
n_o3p_y	3^1A_1	11.25	2^3A_1	11.05
n_o3p_z	2^1B_2	11.20	2^3B_2	11.01
$n_o3d_{z^2}$	3^1B_2	11.82	3^3B_2	11.82
$n_o3d_{x^2-y^2}$	4^1B_2	11.88	4^3B_2	11.80
n_o3d_{xz}	4^1A_2	11.94	3^3A_2	11.97
n_o3d_{yz}	4^1A_1	11.98	4^3A_1	11.88
	π Rydberg States			
$\pi3s$	1^1B_1	10.67	1^3B_1	10.20
$\pi3p_x$	5^1A_1	12.19	3^3A_1	11.98
$\pi3p_y$				
$\pi3p_z$	3^1B_1	12.41	3^3B_1	12.42
$\pi3d_{z^2}$	4^1B_1	12.84	4^3B_1	12.75
$\pi3d_{x^2-y^2}$	5^1B_1	13.26	5^3B_1	13.15
$\pi3d_{xz}$	6^1A_1	13.25	5^3A_1	13.19

(3) C−O Potential Curves for F_2CO. Keeping the CF distance and the FCF angle at GS equilibrium values, energies were calculated for CO distances from 2.0 to 3.6 or 3.8 a_0, with

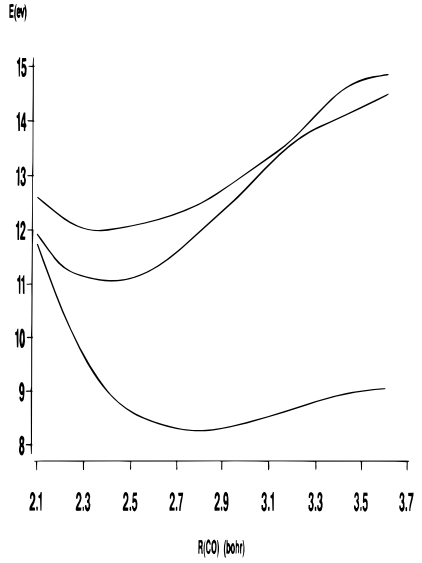

Figure 1. C−O potential curves for 2^1A_1 to 4^1A_1 states of F_2CO. The states are, in order, $\pi\pi^*$, n_o3p_y, and n_o3d_{yz}. After the avoided crossing at 3.2 b, the ordering is $\pi\pi^*$, $\pi3p_x$, and n_o3p_y.

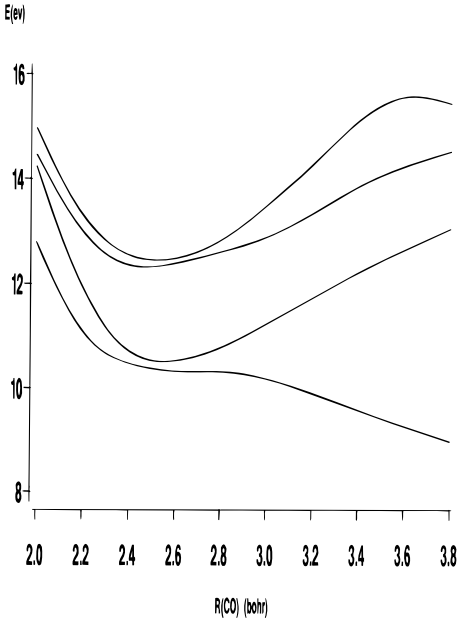

Figure 2. C−O potential curves for 1^1B_1 to 4^1B_1 states of F_2CO. At 2.2 b, the states are, in order, $\pi3s$, $\sigma\pi^*$, $\pi3p_z$ and $\pi3d_{z^2}$. At 3.2 b, they are $\pi\sigma^*$, $\sigma\pi^*$, $\pi3s$, and $\pi3p_z$.

four roots each, using basis set A. Extrapolated energies will be given.

In Figures 1−4, the CO potential curves are shown for singlet A_1, B_1, B_2, and A_2 states, respectively. R_{CO}, T_e, and ν_{CO} values, obtained for these restricted optimizations and therefore labeled with a prime, are given in Table 7.

In Figure 1, for $^1A_1$ states, the GS potential has been omitted. From about 3 a_0 on, the $\pi\pi^*$ configuration mixes with the GS configuration n_o^2. Correspondingly, 2^1A_1, being $\pi\pi^*$ at lower R, starts mixing with n_o^2. At 3.8 a_0, X^1A_1 is 27% n_o^2 and 56% $\pi\pi^*$, whereas 2^1A_1 is 44% n_o^2 and 30% $\pi\pi^*$. So at this distance, the two states have already interchanged their leading configurations. 3^1A_1 and 4^1A_1 are the n_o3p_y and n_o3d_{yz} Rydberg states, respectively. The $\pi\pi^*$ potential crosses the lower of these Rydberg states around 2.1 a_0. Starting at about 2.8 a_0, 4^1A_1 changes from n_o3d_{yz} to $\pi3p_x$, and $\pi3p_x$ crosses n_o3p_y around 3.2 a_0.

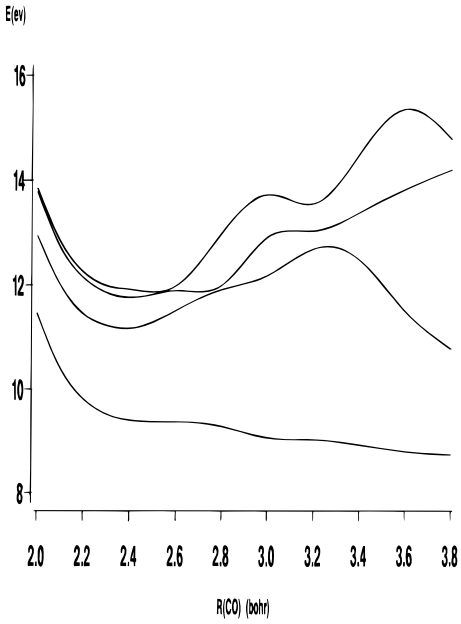

Figure 3. C−O potential curves for 1^1B_2 to 4^1B_2 states of F_2CO. At 2.2 b, the states are, in order, n_o3s, n_o3p_z, $n_o3d_{z^2}$, and $n_o3d_{x^2-y^2}$. At 3.4 b, they are $n_o\sigma^*$, $\pi n_o\pi^*\sigma^*$, n_o3s, and n_o3p_z.

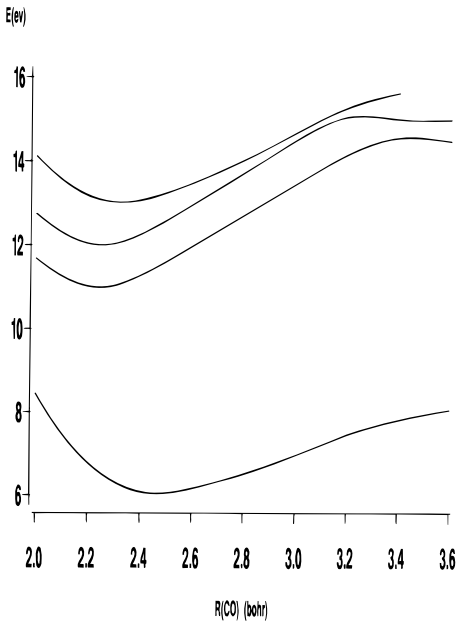

Figure 4. C−O potential curves for 1^1A_2 to 4^1A_2 states of F_2CO. The ordering of states is $n_o\pi^*$, n_o3p_x, n_o3d_{xz}, and $\pi3p_y$.

The $^1B_1$ potentials show several avoided crossings. Around 2.2 a_0, the ordering of states is $\pi3s$, $\sigma\pi^*$, $\pi3p_z$, and $\pi3d_{z^2}$, which is mixed with $\pi\sigma^*$. At larger CO distances, say 3.2 a_0, the lowest state is $\pi\sigma^*$ followed by $\sigma\pi^*$ (bound), $\pi3s$, and $\pi3p_z$. As seen, $\pi3s$ is strongly perturbed by its interaction with $\sigma\pi^*$ and $\pi\sigma^*$ in the 2.3−2.6 Å region. The repulsive $\pi\sigma^*$ state, the highest-lying state at short distances, crosses through $\pi3p_z$, $\sigma\pi^*$, and $\pi3s$ to become the lowest state at large distances. It leads to the dissociation $F_2CO \rightarrow CF_2 + O$.

The Rydberg MO which is mainly $3d_{z^2}$ at small R_{CO} changes gradually into σ^* as R_{CO} increases.

The $^1B_2$ potentials look complicated but are actually fairly easy to understand. Around 2.2 a_0, one sees, in order of increasing energy, the Rydberg states n_o3s, n_o3p_z, $n_o3d_{z^2}$, and $n_o3d_{x^2-y^2}$. These Rydberg potentials are crossed by two repulsive

TABLE 7: Adiabatic (Restricted) Values T_e', R_{CO}', and ν_{CO}', Derived from CO Potentials of F_2CO, Using Basis Set A

state	config	T_e' (eV)[a]	R_{CO}' (a_0)[a]	ν_{CO}' (cm^{-1})[b]
1^1A_1	GS	0.00	2.20	1942[c]
2^1A_1	$\pi\pi^*$	8.55	2.80	980
3^1A_1	n_o3p_y	11.20	2.40	1460
4^1A_1	n_o3d_{yz}	12.00	2.40	1465
1^1B_1	$\pi3s/\pi\sigma^*$	repulsive		
2^1B_1	$\sigma\pi^*$	~10.4	~2.55	1825
3^1B_1	$\pi3p_z$	12.30	2.45	1445
4^1B_1	$\pi3d_{z^2}$	12.45	2.50	1485
1^1B_2	$n_o3s/n_o\sigma^*$	repulsive		
2^1B_2	n_o3p_z	11.15	2.40	1605
3^1B_2	$n_o3d_{z^2}$	11.75	2.40	1730
4^1B_2	$n_o3d_{x^2-y^2}$	11.85	2.50	1285
1^1A_2	$n_o\pi^*$	6.05	2.60	1190
2^1A_2	n_o3p_x	10.95	2.35	1630
3^1A_2	n_o3d_{xz}	11.95	2.35	1565
4^1A_2	$\pi3p_y$	13.00	2.45	1170

[a] Values rounded off to nearest 0.05. [b] Values rounded off to nearest 5. [c] Matched to experimental value. See text.

potentials: between 2.5 and 2.8 a_0 by $n_o\sigma^*$ and at larger R by the four-open-shell configuration $\pi n_o\pi^*\sigma^*$. At 2.9 a_0, for example, the ordering of states is $n_o\sigma^*$, n_o3s, n_o3p_z, and $n_o3d_{z^2}$. At 3.4 a_0, $n_o\sigma^*$ is followed by $\pi n_o\pi^*\sigma^*$, n_o3s, and n_o3p_z. The crossing of $n_o\sigma^*$, a repulsive state leading again to dissociation of F_2CO into $CF_2 + O$, prevents n_o3s from having a minimum and greatly distorts the potential functions of n_o3p_z and $n_o3d_{z^2}$. At 3.6 a_0, 4^1B_2 shows the beginning of another repulsive state with four open shells. As mentioned in the case of $^1B_1$ states, the $3d_{z^2}$ MO changes from Rydberg character at small R_{CO} to σ^* character at larger R_{CO}.

Finally, the $^1A_2$ potentials are straightforward. At small distances, $n_o\pi^*$ is followed by n_o3p_x, n_o3d_{xz}, and $\pi3p_y$. Starting at 3.4 a_0, the Rydberg potentials are crossed by the repulsive four-open-shell state $\sigma n_o\pi^*\sigma^*$.

For calculating the CO frequencies given in Table 7, the GS frequency was matched to the experimental number, 1942 cm^{-1}, thereby obtaining an effective reduced mass. The given frequencies have to be taken with caution, since they all correspond to CF distances and FCF angles fixed at GS equilibrium values. The notation ν_{CO}' should remind the reader of this limited approach.

(4) C−F Potential Curves for F_2CO. While C_{2v} symmetry was retained, potential energies were calculated for CF distances ranging from 2.2 to 3.4 a_0. In all cases, R_{CO} and the FCF angle were kept at the experimental values of 2.211 a_0 and 107.6°, respectively. Basis set A was used. Extrapolated energies for four roots will be given.

In Figures 5−8, the CF potentials are shown for $^1A_1$, $^1B_1$, $^1B_2$, and $^1A_2$ states, respectively. In Table 8, restricted adiabatic values T_e', R_{CF}', and ν_{CF}' are given. The ν_{CF} frequencies correspond to the A_1-symmetric CF stretch of F_2CO and have been matched to the GS experimental value of 965 cm^{-1}.[35]

The most striking feature about all CF potential curves is the crossing by strongly repulsive potentials at larger R values, leading in many instances to a second minimum.

Around 2.4 a_0, the $^1A_1$ potentials have the ordering GS (not shown in Figure 5), $\pi\pi^*$, n_o3p_y, and n_o3d_{yz}. The $\pi\pi^*$ potential crosses n_o3p_y at about 2.3 a_0. The repulsive potential that crosses all states, except for the GS, between 3.0 and 3.2 a_0 is $\sigma\sigma^*$. After the crossing, at 3.4 a_0, the ordering of states is GS, $\sigma\sigma^*$, $\pi\pi^*$, and $n_{b1}\pi^*$. The latter state, not seen at smaller distances, mixes heavily with $\pi\pi^*$ and $n_{a1}\sigma^*$. The 2^1A_1 state, which is $\sigma\sigma^*$ at large distances, appears to have a minimum around 3.3 a_0. The minima of 3^1A_1 and 4^1A_1, around 3.2 a_0, are caused by avoided crossings.

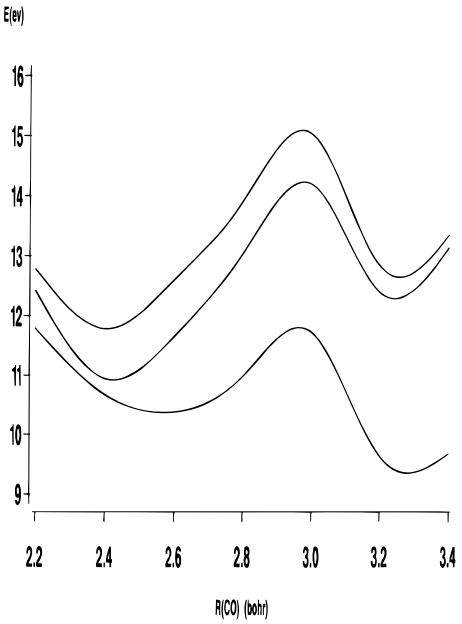

Figure 5. C−F potential curves for 2^1A_1 to 4^1A_1 states of F_2CO. At 2.4 b, the states are, in order, $\pi\pi^*$, n_o3p_y, and n_o3d_{yz}. At 3.4 b, they are $\sigma\sigma^*$, $\pi\pi^*$, and $n_{b1}\pi^*$.

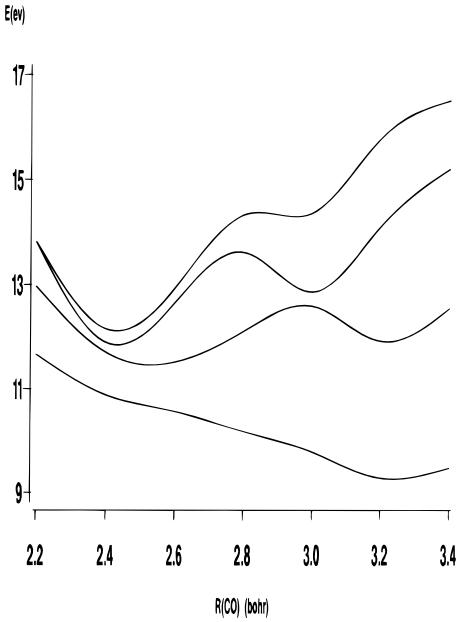

Figure 6. C−F potential curves for 1^1B_1 to 4^1B_1 states of F_2CO. At 2.4 b, the states are, in order, $\pi3s$ mixed with $\pi\sigma^*$, $\sigma\pi^*$, $\pi3p_z$, and $\pi3d_{z^2}$. At 3.2 b, they are $\pi\sigma^*$, $n_{b1}\sigma^*$, $\sigma\pi^*$, and $\pi3p_z$.

For the $^1B_1$ states, the ordering at 2.2 a_0 is $\pi3s$, $\pi3p_z$, $\pi3d_{z^2}$, and $\sigma\pi^*$. The lowest state 1^1B_1 changes into $\pi\sigma^*$ and is mainly dissociative, but a shallow minimum is formed around R_{CF} = 3.2 a_0. The $\sigma\pi^*$ potential, having the highest energy at R_{CF} = 2.2 a_0, crosses through $\pi3p_z$ and $\pi3d_{z^2}$ and develops a minimum at R_{CF} = 2.55 a_0, with T_e' = 11.45 eV. Between 2.4 and 2.8 a_0, the sequence of states is $\pi\sigma^*$, $\sigma\pi^*$, $\pi3p_z$, and $\pi3d_{z^2}$. At distances above 2.8 a_0 the $\sigma\pi^*$ and $\pi3p_z$ potentials are crossed by $n_{b1}\sigma^*$ (or $\pi'\sigma^*$, π' being a lower-energy π-type MO), which again appears to develop a long-range minimum. Therefore, at 3.2 a_0, $\pi\sigma^*$ is followed by $n_{b1}\sigma^*$, $\sigma\pi^*$, and $\pi3p_z$. The only problem with this interpretation of potential curves is the apparent disappearance of $\pi3s$. Although clearly present at small R_{CF},

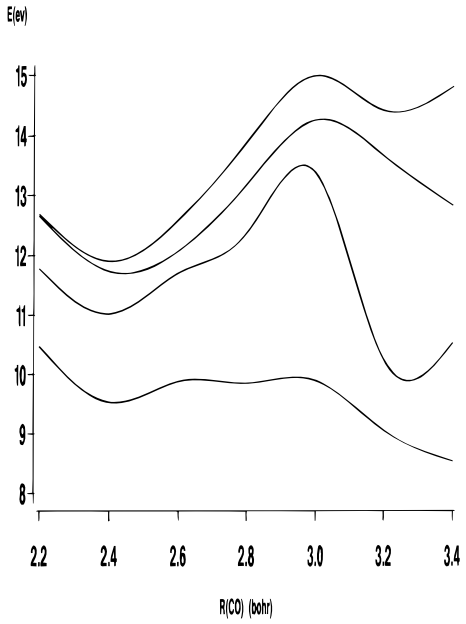

Figure 7. C−F potential curves for 1^1B_2 to 4^1B_2 states of F_2CO. At 2.4 b, the states are, in order, n_o3s, n_o3p_z, $n_o3d_{z^2}$, and $n_o3d_{x^2-y^2}$. At 2.8 b, they are $n_o\sigma^*$, n_o3s, n_o3p_z, and $n_o3d_{z^2}$. The strongly repulsive state at around 3 b is $n_{b2}\sigma^*$.

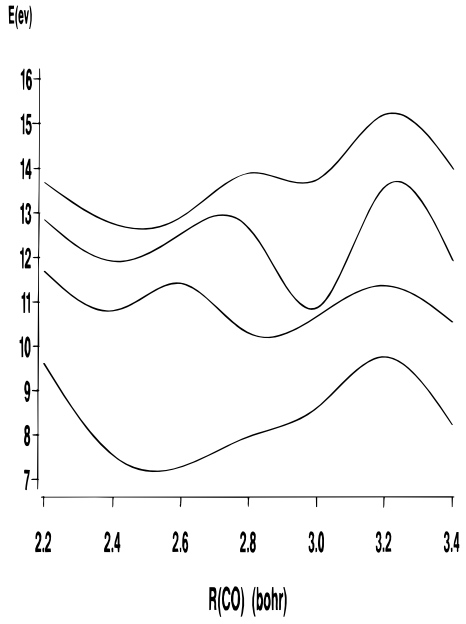

Figure 8. C−F potential curves for 1^1A_2 to 4^1A_2 states of F_2CO. At 2.4 b, the states are, in order, $n_o\pi^*$, n_o3p_x, n_o3d_{xz}, and $\pi3p_y$. At 3.4 b, they are $n_{a2}\sigma^*$, $n_o\pi^*$, $n_{b2}\pi^*$, and $n_{b2}'\pi^*$.

the Rydberg MO changes into σ^* for larger distances, as seen earlier, and the 3s Rydberg character gets mixed into $\pi3p_z$. On the basis of orbital composition and mixing of configurations, $\pi3p_z$ at larger distances may be relabeled into $\pi3s$ and, in turn, $\pi3d_{z^2}$ into $\pi3p_z$.

The $^1B_2$ potentials in Figure 7 have, at short distances, n_o3s followed by n_o3p_z, $n_o3d_{z^2}$, and $n_o\sigma^*$. The last state, $n_o\sigma^*$, crosses through the Rydberg potentials to assume the lowest-state position, say at 2.8 a_0, where it is followed by n_o3s, n_o3p_z, and $n_o3d_{z^2}$. Between 2.9 and 3.2 a_0, all potentials are crossed by the repulsive $n_{b2}\sigma^*$, causing a minimum for 2^1B_2 around 3.3 a_0 due to the avoided crossing.

TABLE 8: Adiabatic (Restricted) Values T_e', R_{CF}', and ν_{CF2}', Derived from CF Potentials of F_2CO, Using Basis Set A

state	config	T_e'(eV)[a]	R_{CF}' (a_0)[a]	ν_{CF2}' (cm^{-1})[b]
1^1A_1	GS	0.0	2.50	965[c]
2^1A_1	$\pi\pi^*$	10.35	2.55	745
3^1A_1	n_o3p_y	10.95	2.40	1140
4^1A_1	n_o3d_{yz}	11.80	2.40	1100
1^1B_1	$\pi3s/\pi\sigma^*$	repulsive		
2^1B_1	$\sigma\pi^*$	11.45	2.55	735
3^1B_1	$\pi3p_z$	11.90	2.40	1255
4^1B_1	$\pi3d_{z^2}$	12.15	2.40	1200
1^1B_2	n_o3s	9.50	2.45	880
2^1B_2	n_o3p_z	11.00	2.35	1025
3^1B_2	$n_o3d_{z^2}$	11.70	2.45	850
4^1B_2	$n_o3d_{x^2-y^2}$	11.90	2.40	980
1^1A_2	$n_o\pi^*$	7.20	2.55	950
2^1A_2	n_o3p_x	10.80	2.40	960
3^1A_2	n_o3d_{xz}	11.90	2.35	1090
4^1A_2	$\pi3p_y$	12.70	2.45	790

[a] Rounded off to the nearest 0.05. [b] Rounded off to the nearest 5. [c] Matched to experimental value. See text.

Contrary to the $^1B_1$ potentials, the 3s Rydberg state n_o3s ($\pi3s$ for $^1B_1$) shows a minimum and can be followed at larger CF distances.

At 3.3 a_0, the ordering of states is $n_{b2}\sigma^*$, $n_o\sigma^*$, $n_{b2}'\sigma^*$, and n_o3s, where n_{b2}' is an orbital below n_{b2} ($3b_2$). The orbital characters, especially of the a_1 MO's, are changing greatly as one goes to larger CF distances.

The ordering of the $^1A_2$ states at 2.4 a_0 is $n_o\pi^*$, n_o3p_x, n_o3d_{xz}, and $\pi3p_y$. Starting at 2.6 a_0, n_o3p_x and $n_o\pi^*$ are crossed by the (up to 3.4 a_0) repulsive $n_{a2}\sigma^*$. From about 2.8 a_0 on, the n_o3p_x, n_o3d_{xz}, and $\pi3p_y$ states are crossed by $n_{b2}\pi^*$ and $n_{b2}'\pi^*$, both of which appear to be stable, with minima in the 3−3.2 a_0 region. At 3.4 a_0, the ordering of states is $n_{a2}\sigma^*$, $n_o\pi^*$, $n_{b2}\pi^*$, and $n_{b2}'\pi^*$. Minima should be formed at 3.4 a_0 or higher for all these states except the lowest one.

(5) FCF Potential Curves for F_2CO. Again, while C_{2v} symmetry is maintained, singlet potential curves were calculated as a function of the FCF angle (at equilibrium, ϕ(FCF) = 107.6°). R_{CO} and R_{CF} were kept at GS equilibrium values. Basis set A was used, and extrapolated energies are given.

Figures 9−12 show the FCF potential curves for the four symmetry species.

The curves for $^1A_1$ are unremarkable, showing the minima of $\pi\pi^*$ and n_o3p_y in the 110° range, whereas the minimum of n_o3d_{yz} is shifted toward 120°.

The $^1B_1$ curves, Figure 10, show two special features. No minimum is obtained for 1^1B_1, which is $\pi3s/\pi\sigma^*$. It may be recalled that $\pi\sigma^*$ is dissociative toward larger R_{CO} (Figure 2) and R_{CF} (Figure 6) values. A move of the equilibrium (if it exists) in the direction of larger FCF angles indicates dissociation of this state to the atomic products C + O + 2F. The 2^1B_1 state, $\sigma\pi^*$, has its minimum between 110 and 120°, as is also the case for the two Rydberg states $\pi3p_z$ and $\pi3d_{z^2}$. Somewhat unexpected is the avoided crossing of $\pi3p_z$ with $\pi3d_{z^2}$ around 130°, after which angle $\pi3p_z$ lies above $\pi3d_{z^2}$.

The $^1B_2$ potentials show again the lowest state being dissociative, moving toward larger FCF angles. Both the R_{CO} and R_{CF} potentials showed this state, which is n_o3s in the region of GS R_{CO} and R_{CF} values and becomes $n_o\sigma^*$ toward larger R_{CO} and R_{CF}, to be dissociative. Again, the preliminary indication, based on the potential curves shown here, is dissociation to C + O + 2F. However, more extensive potential surfaces are needed to settle this point. The three higher-lying states, n_o3p_z, $n_o3d_{z^2}$, and $n_o3d_{x^2-y^2}$, have avoided crossings around 110° and 130°, again quite unexpectedly.

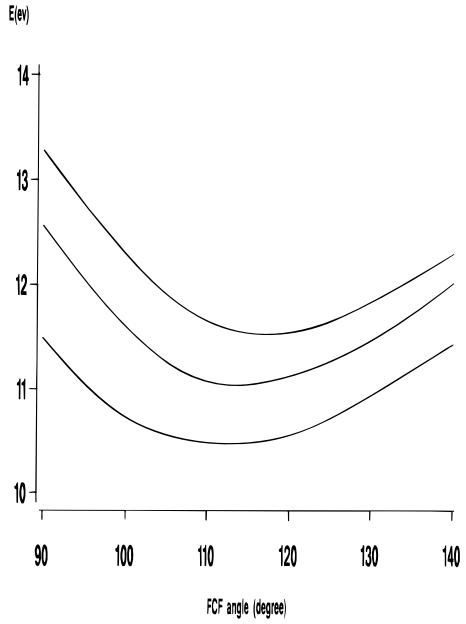

Figure 9. FCF angle potential curves for 2^1A_1 to 4^1A_1 states of F_2CO. The states are, in order, $\pi\pi^*$, n_o3p_y, and n_o3d_{yz}.

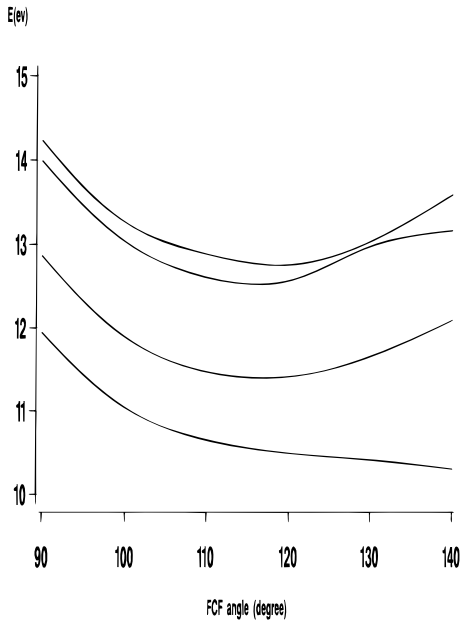

Figure 10. FCF angle potential curves for 1^1B_1 to 4^1B_1 states of F_2CO. The states are, in order, $\pi3s/\pi\sigma^*$, $\sigma\pi^*$, $\pi3p_z$, and $\pi3d_{z^2}$. After 130°, $\pi3d_{z^2}$ lies below $\pi3p_z$.

The $^1A_2$ potentials, Figure 12, have well-established minima between 120 and 125° for $n_o\pi^*$, n_o3p_x, n_o3d_{xz}, and $\pi3p_y$. At angles around 100°−110°, $n_{b2}\pi^*$, not seen at angles above 110°, crosses $\pi3p_y$, n_o3d_{xz}, and n_o3p_x from above and settles as the 2^1A_2 state for angles below 100°. It may be noted that $n_{b2}\pi^*$ is listed as state 3^1A_2 in Table 4, which gives the vertical excitation energies. Apparently, the two basis sets, basis set A used in the present figures and basis set B used for the vertical excitation energies, correspond to a small shift in the FCF angle. In Figure 12, at 110°, the ordering of $^1A_2$ states is $n_o\pi^*$, n_o3p_x, n_o3d_{xz}, and $\pi3p_y$, identical to the ordering in the R_{CO} and R_{CF} potentials, all calculated with basis set A, whereas at 100° the ordering is $n_o\pi^*$, n_o3p_x, $n_{b2}\pi^*$, and n_o3d_{xz}, agreeing with that given in Table 4 for which basis set B was used. At 90°, the second state is $n_{b2}\pi^*$ followed by n_o3p_x and n_o3d_{xz}.

(6) CI Results for F_2CO^+ and Ionization Potentials of

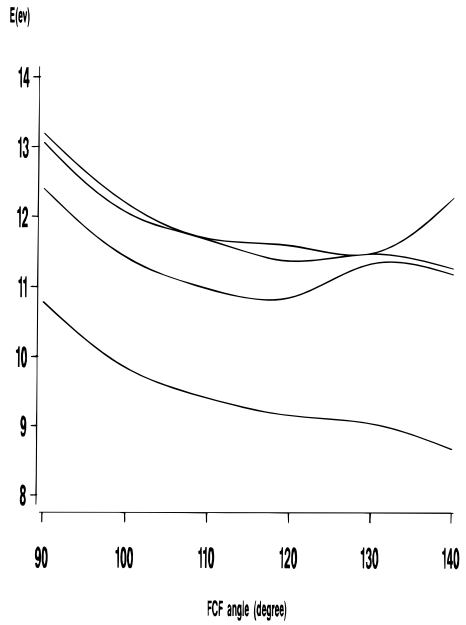

Figure 11. FCF angle potential curves for 1^1B_2 to 4^1B_2 states of F_2CO. The states are, in order, $n_o3s/n_o\sigma^*$, n_o3p_z, $n_o3d_{z^2}$, and $n_o3d_{x^2-y^2}$, with avoided crossings and corresponding changes in ordering above 130°.

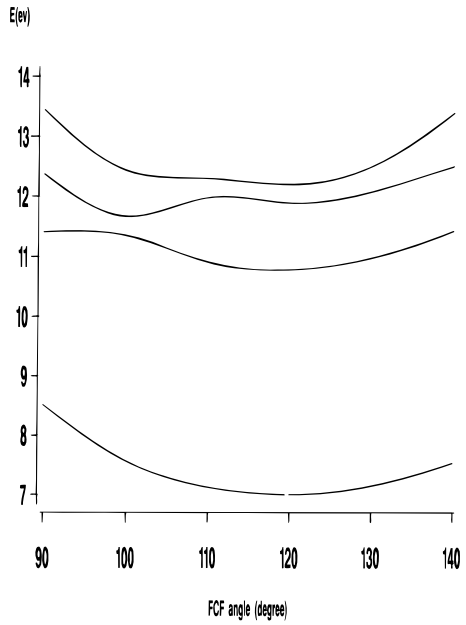

Figure 12. FCF angle potential curves for 1^1A_2 to 4^1A_2 states of F_2CO. At 120°, the states are, in order, $n_o\pi^*$, n_o3p_x, n_o3d_{xz}, and $\pi3p_y$. At 90°, they are $n_o\pi^*$, $n_{b2}\pi^*$, n_o3p_x, and n_o3d_{xz}.

F_2CO. Using basis set B, CI calculations were performed for the two lowest $^2A_1$, $^2B_1$, $^2B_2$, and $^2A_2$ states of F_2CO^+, at the GS geometry of F_2CO. Additional CI calculations were done for $^2B_1$ and $^2B_2$ states at their respective optimized geometry as given in Table 3.

Energy differences relative to the GS of F_2CO at its equilibrium geometry are given in Table 9. ΔE values obtained for low-lying states of F_2CO^+ at the F_2CO GS geometry are vertical ionization potentials (IP_v) of F_2CO, whereas the lowest $\Delta E'$ values, obtained for F_2CO^+ at their respective optimized geometry (13.73 and 12.81 eV), are adiabatic IP's (IP_a). The $\Delta E'$ values for higher $^2B_2$ states relate to vertical excitation energies of F_2CO^+.

In Table 10, calculated vertical and adiabatic ionization

TABLE 9: CI Energies of F_2CO^+, Calculated at the GS Geometry of F_2CO (ΔE Values) and at the Optimized 1^2B_1, X^2B_2 Geometries, Respectively ($\Delta E'$ Values)

state	ΔE (eV)	config	$\Delta E'$ (eV)
1^2A_1	17.00	$\sigma \rightarrow \infty$	
2^2A_1	19.19	$\sigma' \rightarrow \infty$	
3^2A_1	22.92	$\sigma'' \rightarrow \infty$	
4^2A_1	24.26	$n_o,n_{a2} \rightarrow \pi^*,\infty$	
1^2B_1	14.65	$\pi \rightarrow \infty$	13.73
2^2B_1	19.92	$\pi' \rightarrow \infty$	21.68
3^2B_1	23.06	$n_o,n_{b2} \rightarrow \pi^*,\infty$	22.83
4^2B_1	23.32	$n_o,n_{b2} \rightarrow \pi^*,\infty$	23.29
1^2B_2	13.45	$n_o \rightarrow \infty$	12.81
2^2B_2	16.70	$n_{b2} \rightarrow \infty$	18.59
3^2B_2	21.15	$n_{b2}' \rightarrow \infty$	21.96
4^2B_2	23.20	$n_o,\pi \rightarrow \pi^*,\infty$	22.45
1^2A_2	17.35	$n_{a2} \rightarrow \infty$	
2^2A_2	24.30	$n_o,\sigma \rightarrow \pi^*,\infty$	
3^2A_2	24.98	$n_{a2},\pi \rightarrow \pi^*,\infty$	
4^2A_2	25.06	$n_o,\sigma \rightarrow \pi^*,\infty$	

TABLE 10: Calculated CI Values for Vertical (IP_v) and Adiabatic (IP_a) Ionization Potentials of F_2CO (in eV) and Comparison with Experimental Results[a]

config	MO	state	IP_v calcd	IP_v exptl	IP_a calcd	IP_a exptl	$-0.92 \times \epsilon_{MO}$
$n_o \rightarrow \infty$	$5b_2$	1^2B_2	13.45	13.6	12.81	13.02	14.1
$\pi \rightarrow \infty$	$2b_1$	1^2B_1	14.65	14.6	13.73	14.09	14.5
$n_{b2} \rightarrow \infty$	$4b_2$	2^2B_2	16.70	16.6[c]		16.1[c]	17.7
$\sigma \rightarrow \infty$	$8a_1$	1^2A_1	17.00	17.2[c]	16.99[b]	16.9[c]	17.7
$n_{a2} \rightarrow \infty$	$1a_2$	1^2A_2	17.35				18.2
$\sigma' \rightarrow \infty$	$7a_1$	2^2A_1	19.19	19.15		19.15	20.1
$\pi' \rightarrow \infty$	$1b_1$	2^2B_1	19.92	19.8			20.5
$n_{b2}' \rightarrow \infty$	$3b_2$	3^2B_2	21.15	21.1			21.7
$\sigma' \rightarrow \infty$	$6a_1$	4^2A_1	22.92	23.4		~22.7	24.0

[a] Vertical excitation energies of F_2CO^+, relative to 12.81 eV, are 5.78, 9.15, and 9.64 eV for 2^2B_2 to 4^2B_2. [b] Value from geometry optimization; see Table 3. [c] Reordered, following calculated results.

potentials are compared with experimental values of Brundle et al.[37] It is seen that calculated vertical IP's agree closely (within 0.2 eV) with their experimental counterpart, provided that the $4b_2/8a_1$ assignment is interchanged. Brundle et al. based their assignments on calculated orbital energies. Their values (factor 0.92) are 17.7 eV for $8a_1$ and 18.0 eV for $4b_2$. Our orbital energies (again multiplied by 0.92), given in the last column of Table 10, are 17.7 eV for both $8a_1$ and $4b_2$, not allowing by themselves a distinction. However, the CI values clearly favor $4b_2$ as having the lower vertical ionization potential, observed at 16.6 eV and calculated to be 16.7 eV, and favor $8a_1$ to be higher, observed at 17.2 eV and calculated to be 17.0 eV. This way, all calculated vertical IP's except for the last one in Table 10 lie within 0.2 eV of the experimental values. A further confirmation of this reassignment comes from the calculated adiabatic value for $8a_1$, taken from Table 3 and mentioned at the end of section 3.1. This value is 16.99 eV, in close agreement with 16.9 eV and not with 16.1 eV. No calculated adiabatic IP is available for $4b_2$, since it corresponds to the second B_2 state for which no SCF or MP2 geometry optimization can be performed. For the last entry of Table 10, $6a_1$, calculated and experimental IP_v's differ by 0.5 eV. Although this deviation may be due to lack of accuracy in the calculations, it is noted that according to Table 9 several ionization processes combined with excitation processes occur around 23 eV. For example, at 23.06 eV, the combined process ($n_o \rightarrow \infty$, $n_{b2} \rightarrow \pi^*$) is listed, and at 23.20 as well as 23.32 eV ($n_o \rightarrow \infty$, $\pi \rightarrow \pi^*$). More such combination processes follow in the 24 eV region.

Adiabatic ionization potentials for $5b_2$ and $2b_1$ were calculated both at the MP2 level, in conjunction with the geometry optimization, and at the CI level, using the MP2 optimized geometries. For $5b_2$ the MP2 value is 12.79 eV, very close to the CI value of 12.81 eV. For $2b_1$, however, the MP2 value (13.93 eV) and the CI value (13.73 eV) differ by 0.2 eV, causing a CI deviation of 0.35 eV from the experimental result.

In footnote a of Table 10, vertical excitation energies for the lowest $^2B_2$ states of F_2CO^+ are given, as calculated from $\Delta E'$ values of Table 9.

Discussion

(1) UV Spectrum of F_2CO. Assignment of the first absorption system of F_2CO, observed between 5.03 and 6.95 eV, to the singlet $n_o \rightarrow \pi^*$ excitation is generally accepted. Theoretical calculations place $T_e(n_o\pi^*)$ around 4.7 eV,[19] which compares well with the experimental T_o of 4.86 eV.[16]

The calculations presented in this paper have been carried out for planar symmetry only. The vertical excitation energy for 1^1A_2 is 7.35 eV. CO potentials lead to $T_e' = 6.05$ eV (Table 7), and full C_{2v} geometry optimizations, as reported by Francisco et al.,[19] give 5.6−6 eV, depending on the method used. Therefore, the 6−7 eV portion of system I is consistent with energies calculated for planar F_2CO.

It might be mentioned here that the central barrier of 8200 cm^{-1} (about 1.02 eV), as derived by Judge and Moule,[16] agrees reasonably well with calculated values. Setting $T_e(C_s) = 4.55$ eV, $T_e(C_{2v})$ should then be about 5.6 eV, as obtained above.

The second system, ranging from 7.02 to 7.66 eV with a maximum at 7.34 eV, shows 20 vibrational bands. Its structure is similar to that of system I, and WD tentatively proposed as the upper state a second $^1A_2$ state, resulting from $n_{b2} \rightarrow \pi^*$, where n_{b2} is (as said earlier) the lone-pair b_2 MO localized on the F's. However, this orbital is at much lower energy than n_o (see Table 2), and according to Table 4, the $n_{b2}\pi^*$ state has a vertical excitation energy of 11.72 eV, about 4.5 eV higher than $n_o\pi^*$. The vibrational progressions in system II can be correlated with frequencies of 500 cm^{-1} (ν_3') and 719 cm^{-1} (ν_2'), assuming a forbidden electronic transition, or alternatively with frequencies of about 1020 cm^{-1} (ν_1') and 719 cm^{-1} (ν_2'), assuming an allowed electronic transition.

Since the calculated vertical excitation energy of the second lowest singlet state is 9.47 eV for 1^1B_2 (n_o3s), with an adiabatic energy certainly not lower than 8.5 eV (see later), we have no choice but to agree with VG in assigning system II to $1^3A'$, the triplet $\pi\pi^*$ state. For this state, the vertical excitation energy is 7.36 eV (Table 5) and T_e is 5.15 eV according to ref 19, with $R_{CO} = 2.650\ a_0$ and $R_{CF} = 2.513\ a_0$. As expected, R_{CO} has increased strongly (by 0.44 a_0) relative to R_{CO} of the GS, whereas R_{CF} has remained essentially constant.

MP2/6-311G* calculations performed by us on $1^3A'(\pi\pi^*)$ give $R_{CO} = 2.640\ a_0$, $R_{CF} = 2.496\ a_0$, and $T_e = 5.22$ eV. The MP2/6-311G* frequencies for $^3(\pi\pi^*)$ are 531.6 (A′, 5.1), 541.5 (A″, 0.8), 659.8 (A′, 19.7), 1082.4 (A′, 39.7), 1257.2 (A″, 255.8), and 1271.5 (A″, 369.4), with IR intensities, in km/mol, given in parentheses. Excitation to $^3(\pi\pi^*)$ would require spin−orbit coupling of $^3(\pi\pi^*)$ with an appropriate singlet state. Since both $^3(\pi\pi^*)$ and $^1(\pi\pi^*)$ are nonplanar, the spin−orbit operator couples these two states in C_s symmetry (but not in C_{2v}). Even small coupling of $^3(\pi\pi^*)$ with $^1(\pi\pi^*)$ would greatly improve the transition moment between the ground state and $^3(\pi\pi^*)$ because of the large oscillator strength associated with $^1(\pi\pi^*)$. In planar symmetry, $^1B_1$ and $^1B_2$ states also couple with $^3(\pi\pi^*)$, but according to Table 4, most have a small oscillator strength and thus are unable to improve that of $^3(\pi\pi^*)$ by much.

System III, observed between 8.13 and 8.52 eV, shows five vibrational bands. The maximum lies at 8.42 eV. It had previously been assigned to $n_o \rightarrow \sigma^*$ or $n_o \rightarrow 3s$. We tentatively support the $n_o \rightarrow 3s$ assignment. Calculations presented earlier give a vertical excitation energy of 9.47 eV for $n_o \rightarrow 3s$. Owing to an avoided crossing of n_o3s with the repulsive $n_o\sigma^*$ in the R_{CO} potentials (Figure 3) that happens just around the minimum R_{CO} of n_o3s, this state develops no potential well. Diabatically, the minimum of n_o3s is estimated to lie at 9.4 eV. The R_{CF} potentials (Figure 7) show a small potential well for n_o3s, with $T_e' = 9.5$ eV (no energy lowering relative to ΔE). CF potential curves (calculations in progress) for R_{CO} values greater than R_{CO} of the GS show an energy stabilization of n_o3s with a more pronounced potential well. For example, fixing R_{CO} at 2.4 a_0 gives an n_o3s minimum at an R_{CF} value of about 2.4 a_0, with an energy of 8.8 eV. This shift to larger R_{CO} probably results from mixing of n_o3s with $n_o\sigma^*$.

The frequency associated with the broad bands of system III is $\nu_2' = 779$ cm^{-1}, the symmetric bend. It was mentioned earlier that the angular plots, Figure 11, show no minimum for 1^1B_2, with the energy decreasing for larger FCF angles. The lowest energy (8.6 eV) is obtained for FCF = 140°, the limit of the angular range calculated. Obviously, something interesting is happening here, but unfortunately, not enough potential surface data are available to understand this situation. Again, the FCF potentials point to lower energies for $n_o3s/n_o\sigma^*$, bringing the calculated values into the energy range observed for system III.

System IV is a continuum, starting at 8.5 eV with a maximum at 9.42 eV and extending beyond the limit of observation at about 10 eV (82 000 cm^{-1}). Because of its high oscillator strength, system IV can clearly be assigned to $^1(\pi\pi^*)$. Also, the continuum can be explained by the avoided crossing of $^1(\pi\pi^*)$ with the ground state, a feature seen in all carbonyl compounds that have been investigated by theoretical methods. With increasing R_{CO} values, the $\pi\pi^*$ configuration moves gradually from 2^1A_1 to X^1A_1, allowing predissociation of 2^1A_1 into the ground state. A continuous spectrum for the $^1(\pi\pi^*)$ state is expected for all carbonyl compounds and has been confirmed for Cl_2CO.[7]

The vertical excitation energy for 2^1A_1 is 10.18 eV, with $f = 0.25$. The R_{CO} potentials give a T_e' of 8.55 eV at $R_{CO} = 2.80$ a_0 (Table 7), whereas the R_{CF} potentials do not lead to a lower energy for 2^1A_1, owing to the use of $R_{CO} = 2.211$ a_0, the GS R_{CO} value.

The $^1(\pi\pi)^*$ state is, according to calculations presently performed in this laboratory, nonplanar, and preliminary CI geometry optimizations place its minimum at about 6.8 eV, with $R_{CO} \cong 2.8$ a_0 and $R_{CF} \cong 2.45$ a_0. Probably because of unfavorable Franck−Condon factors, the lower vibrational levels of $^1(\pi\pi^*)$ cannot be reached from the GS, confining the observed range to energies above 8.5 eV.

(2) Perfluoro Effect. Brundle et al.[37] observed from photoelectron spectra and MO calculations that in perfluoro compounds the σ-MO's are greatly stabilized (by 2.5−4 eV) compared with corresponding hydrides. Stabilization of π-MO's, however, is quite small.

In carbonyl fluoride, the first vertical IP, $n_o \rightarrow \infty$, is 2.7 eV higher in F_2CO than in H_2CO, or the n_o HOMO of F_2CO is about 2.7 eV more stable than that of H_2CO.

Since we propose for F_2CO a reordering of $4b_2$ and $8a_1$, with IP_v of $4b_2$ at 16.6 eV and IP_v of $8a_1$ at 17.2 eV, the stabilization of F_2CO MO's vs H_2CO MO's is somewhat changed compared to the values given by Brundle et al. In Table 11, observed vertical IP's for F_2CO[37] (and Cl_2CO[38]) are compared with corresponding values for H_2CO.[37] Following Brundle et al., the second b_2 IP of H_2CO, 16.6 eV, is compared with the third b_2 of F_2CO (and Cl_2CO), assuming that the second-highest-occupied b_2 orbital in F_2CO and Cl_2CO is an F or Cl lone-pair MO, which has no equivalent MO in H_2CO. Similarly, the second a_1 IP of H_2CO, at 21.8 eV, is compared with the third a_1 IP of F_2CO. Under these assumptions, it is seen that relative to H_2CO b_2 MO's of F_2CO are stabilized by 2.7−4.5 eV and a_1 MO's by 1.2−1.6 eV, whereas b_1 (π) is hardly changed. The large stabilization of $3b_2$, 4.5 eV, cannot be taken at face value, since the F lone-pair character is not confined solely to the $4b_2$ MO but instead is spread between $4b_2$ and $5b_2$. So the actual stabilization of b_2 MO's is about 2.5−3.5 eV, and that of a_1 MO's is 1−1.5 eV. Still, this "perfluoro effect" is remarkable and can be nicely demonstrated when comparing the IP changes of F_2CO with those of Cl_2CO. Here, no trend in stabilization can be detected except perhaps that ΔIP_v for the b_2 MO's is positive.

TABLE 11: Vertical Ionization Potentials IP_v (in eV) of F_2CO and Cl_2CO, Compared with Corresponding Values of H_2CO[a]

	F_2CO		Cl_2CO		H_2CO
MO[b]	IP_v	ΔIP_v	IP_v	ΔIP_v	IP_v
$5b_2$	13.6	2.7	11.9	1.0	10.9
$2b_1$	14.6	0.1	13.1	−1.4	14.5
$4b_2$	16.6[c]		12.5		
$8a_1$	17.2[c]	1.2	13.5	−2.5	16.0
$1a_2$	17.35[d]		12.7		
$7a_1$	19.15		16.7		
$1b_1$	19.8		16.1		
$3b_2$	21.1	4.5	17.0	0.4	16.6[e]
$6a_1$	23.4	1.6			21.8[f]

[a] Energy differences (ΔIP_v) relative to H_2CO. Experimental values for F_2CO and H_2CO from ref 37, for Cl_2CO from ref 38. [b] Orbital numbering of F_2CO. [c] Reordered; see text. [d] Calculated value. [e] Compared with $3b_2$ of F_2CO, not with $4b_2$, owing to MO character. [f] Compared with $6a_1$ of F_2CO, not with $7a_1$, owing to MO character.

Orbital energies for the HOMO(HO) and HO-1, listed in Table 2 for F_2CO, Cl_2CO, and H_2CO, nicely reflect the trends in IP's.

(3) Vibrational Structure of Photoelectron Spectrum. In the following, the vibrational structure of the photoelectron spectrum of F_2CO, as given by Brundle et al.,[37] will be discussed.

The $5b_2$ band shows a vibrational progression with 1550 and 530 cm^{-1} spacings. The 1550 frequency has been assigned to ν_1' (CO stretch) and 530 to ν_3' (FCF bend) or ν_2' (CF stretch).

Our results in Table 3 indicate that in X^2B_2 of F_2CO^+ R_{CO} has increased by 0.095 Å, R_{CF} has decreased by 0.076 Å, and ϕ(FCF) has increased by about 13°. Such changes in geometry should be accompanied by a rich vibrational structure involving CO and CF stretches as well as FCF bendings. The calculated frequencies of the a_1 symmetric stretch of CO and the b_2 asymmetric stretch of CF are similar, with values of 1694 and 1654 cm^{-1}, respectively (unscaled). Both frequencies may actually be present in the spectrum. The observed 530 cm^{-1} frequency compares best with the calculated 579 cm^{-1} for the symmetric FCF bend, but the asymmetric FCF bend has only a slightly lower frequency.

The $2b_1$ band of the photoelectron spectrum has, as expected, long vibrational progressions, showing frequencies of 1450 cm^{-1} and 970 or ∼500 cm^{-1}.

The geometry changes of 1^2B_1, according to Table 3, relative to the GS of F_2CO, are $\Delta R_{CO} = 0.14$ Å, $\Delta R_{CF} = -0.08$ Å, and $\Delta\phi$(FCF) = 9.6°. The R_{CO} change is most pronounced. Again,

calculated CO and CF frequencies are close, but ν_1(CO) is about 120 cm^{-1} lower than for the X^2B_2 state, confirming that the observed 1450 cm^{-1} frequency is ν_1(CO), compared to the observed value of 1550 cm^{-1} for ν_1(CO) in X^2B_2.

Since the $4b_2$, $8a_1$, and $1a_2$ ionizations lie close together, the observed bands in this energy region could not be clearly assigned. From the calculations, the 16.6−16.8 eV range is probably $4b_2$, the larger peaks starting around 16.9 eV are $8a_1$, and $1a_2$ may be tagged on to the high-energy end of the strong vibronic structure around 17.3 eV.

Table 3 contains data for the 1^2A_1 state of F_2CO^+. Its geometry is remarkably similar to that of the X^2B_2 state, with an increase in R_{CO} and a decrease in R_{CF} relative to the GS of F_2CO. The CO stretch and CF asymmetric stretch frequencies are calculated to be virtually identical.

The geometry of ionic states higher than 1^2A_1, corresponding to $8a_1 \rightarrow \infty$, has not been optimized, and no frequencies were calculated. Therefore, the calculations presented here do not apply to the vibrational structure of higher photoelectron bands.

One might perhaps add that the $1a_2 \rightarrow \infty$ part of the photoelectron spectrum, if seen at all, is expected to be structureless, since $1a_2$ is a perfectly nonbonding MO, only having contributions from the two fluorine atoms.

Summary and Conclusion

By use of multireference CI methods with high-quality basis sets, the four to six lowest states of each symmetry species of F_2CO in C_{2v} symmetry were investigated. Besides vertical excitation energies of both singlet and triplet states, potential energy curves were presented for singlet states as a function of the C−O and C−F distances and as a function of the FCF angle. In each case, the other geometry parameters were kept at ground-state values. The (singlet) valence states $\pi\pi^*$ and $\sigma\pi^*$ and Rydberg states of type $n_o \rightarrow$ 3s, 3p, 3d are stable, although n_o3s mixes strongly with $n_o\sigma^*$, the latter valence state being repulsive. Also, the π-Rydberg states π3s, π3p, and some of the π3d obtained here are stable. The $n_o \rightarrow$ 4s, 4p, 4d Rydberg states were not obtained, since the basis set contained only one set of Rydberg functions (for $n = 3$), and some of them may lie below members of the π-Rydberg series.

The CF potential curves show many secondary minima at larger CF distances (e.g., 3.2 b or 1.7 Å), separated from the minima in the ground-state region by high barriers. The potential curves for varying the FCF angle show dissociative behavior of the $\pi\sigma^*$ and $n_o\sigma^*$ states toward larger angles.

The observed UV system I is confirmed to be $^1(n_o \rightarrow \pi^*)$. The theoretical results leave for system II no other explanation but that it is a triplet $\pi \rightarrow \pi^*$ transition. System III agrees energetically with the $n_o \rightarrow$ 3s transition, which in the equilibrium region mixes with $n_o \rightarrow \sigma^*$. By comparison of the calculated with the observed oscillator strengths, system IV, which is a continuum, is $^1(\pi \rightarrow \pi^*)$. The $^1(\pi\pi^*)$ state is nonplanar, like $^1(n_o\pi^*)$, and will be the subject of further studies.

Calculated MRCI ionization potentials of F_2CO agree closely with observed values but suggest that the $4b_2$ and $8a_1$ assignments be interchanged. Vertical ionization potentials of F_2CO and Cl_2CO are compared with corresponding ones of H_2CO. The perfluoro effect, as discussed by Brundle et al.,[37] is confirmed for the σ MO's of F_2CO in that b_2-type IP's are strongly stabilized. No similar effect could be found for Cl_2-CO.

So far, all calculations on excited states of F_2CO were restricted to C_{2v} symmetry. For the given potential curves, (e.g., as a function of the CO distance), the other geometry parameters (CF distance and FCF angle, for example) were held at GS equilibrium values. The need for potential *surfaces* in C_{2v} symmetry, where two or more parameters are changed simultaneously, was seen in the example of system III. The excitation likely to be involved here is $n_o \rightarrow$ 3s, yet the repulsive CO potential of $^1(n_o\sigma^*)$ crosses that of $^1(n_o3s)$ around its minimum. The problem of the stability of $^1(n_o3s)$ can only be solved by having multidimensional potential surfaces.

Also, out-of-plane potentials are required, whereby the symmetry of the molecule is lowered to C_s. The $^1(\pi\pi^*)$ state, the most important intensity provider to the spectrum of F_2CO, is nonplanar. System II needs, in our interpretation, the involvement of $^1(\pi\pi^*)$ to lend intensity to $^3(\pi\pi^*)$, which via a spin−orbit mechanism can only occur in nonplanar symmetry.

Work on potential energy surfaces, both in C_{2v} and C_s symmetry, is in progress.

Acknowledgment. We are grateful to Michel Hachey for providing literature on F_2CO, for his initial CI calculations, and also for reading the manuscript and commenting on it. Bernd Engels, University of Bonn, kindly provided the direct-CI programs, without which the calculations presented here would not have been possible. Thanks are also extended to Melanie Neil for help with the figures. Financial support by NSERC (Canada) is much appreciated.

References and Notes

(1) Hachey, M. R. J.; Bruna, P. J.; Grein, F. *J. Chem. Soc., Faraday Trans.* **1994**, *90*, 683.
(2) Bruna, P. J.; Hachey, M. R. J.; Grein, F. *J. Phys. Chem.* **1995**, *99*, 16576.
(3) Hachey, M. R. J.; Bruna, P. J.; Grein, F. *J. Phys. Chem.* **1995**, *99*, 8050.
(4) Grein, F.; Hachey, M. R. J. *Int. J. Quantum Chem.* **1996**, *60*, 1661.
(5) Hachey, M. R. J.; Grein, F. *Chem. Phys. Lett.* **1996**, *256*, 179.
(6) Hachey, M. R. J.; Bruna, P. J.; Grein, F. *J. Mol. Spectrosc.* **1996**, *176*, 375.
(7) Hachey, M. R. J.; Grein, F. *Chem. Phys.* **1997**, *224*, 19.
(8) Milligan, D. E.; Jacox, M. E.; Bass, A. M.; Comeford, J. J.; Mann, D. E. *J. Chem. Phys.* **1965**, *42*, 3187.
(9) Workman, G. L.; Duncan, A. B. F. *J. Chem. Phys.* **1970**, *52*, 3204.
(10) Laurie, V. W.; Pence, D. T. *J. Mol. Spectrosc.* **1963**, *10*, 155.
(11) Laurie, V. W.; Pence, D. T.; Jackson, R. H. *J. Chem. Phys.* **1962**, *37*, 2995.
(12) Overend, J.; Scherer, J. R. *J. Chem. Phys.* **1960**, *32*, 1296.
(13) Miller, R. F.; Curl, R. F., Jr. *J. Chem. Phys.* **1961**, *34*, 1847.
(14) Vasudevan, K.; Grein, F. *Int. J. Quantum Chem.* **1978**, *14*, 717.
(15) Robin, M. B. *Higher Excited States of Polyatomic Molecules*; Academic Press: New York, 1975; Vol. 2.
(16) Judge, R. H.; Moule, D. C. *J. Chem. Phys.* **1983**, *78*, 4806.
(17) Brewer, D. A.; Schug, J. C.; Phillips, D. H. *J. Chem. Phys.* **1980**, *73*, 4486.
(18) Kapur, A.; Steer, R. P.; Mezey, P. G. *Can. J. Chem.* **1982**, *60*, 100.
(19) Francisco, J. S.; Li, Z.; Hand, M. R.; Williams, I. H. *Chem. Phys. Lett.* **1993**, *214*, 591.
(20) Francisco, J. S.; Li, Z. *J. Phys. Chem.* **1989**, *93*, 8118.
(21) Francisco, J. S. *Chem. Phys. Lett.* **1994**, *218*, 401.
(22) Li, Z.; Francisco, J. S. *J. Am. Chem. Soc.* **1989**, *111*, 5660.
(23) Sumathi, R.; Chandra, A. K. *Chem. Phys.* **1992**, *165*, 257.
(24) Buenker, R. J.; Peyerimhoff, S. D. *Theor. Chim. Acta (Berlin)* **1974**, *35*, 33.
(25) Buenker, R. J.; Peyerimhoff, S. D. *Theor. Chim. Acta (Berlin)* **1975**, *39*, 217.
(26) Buenker, R. J. *Stud. Phys. Theor. Chem.* **1982**, *21*, 17.
(27) Buenker, R. J.; Peyerimhoff, S. D.; Butscher, W. *Mol. Phys.* **1978**, *35*, 771 and references therein.
(28) Buenker, R. J.; Phillips, R. A. *J. Mol. Struct.: THEOCHEM* **1985**, *123*, 291.
(29) Program provided by B. Engels.
(30) Dunning, T. H. *J. Chem. Phys.* **1971**, *55*, 716.
(31) Dunning, T. H.; Hay, P. J.. In *Modern Theoretical Chemistry*; Schaefer, H. F., Eds.; Plenum Press: New York, 1976; Vol. 3.

(32) Carpenter, J. H. *J. Mol. Spectrosc.* **1974**, *50*, 182.
(33) Nakata, M.; Kohata, K.; Fukuyama, T.; Kuchitsu, K.; Wilkins, C. J. *J. Mol. Struct.* **1980**, *68*, 271.
(34) Frisch, M. J.; Head-Gorden, M.; Trucks, G. W.; Foresman, J. B.; Schlegel, H. B.; Raghavachari, K.; Robb, M. A.; Binkley, J. S.; Gonzalez, C.; Defrees, D. J.; Fox, D. J.; Whiteside, R.; Seeger, R.; Melius, C. F.; Baker, J.; Martin, R. L.; Kahn, L. R.; Stewart, J. J. P.; Topiol, S.; Pople, J. *Gaussian 90*; Gaussian: Pittsburgh, PA, 1990.
(35) Herzberg, G. *Electronic States of Polyatomic Molecules*; Van Nostrand: New York, 1966; Vol. 3.
(36) Kwiatkowski, J. S.; Leszczynski, J. *Mol. Phys.* **1994**, *81*, 119.
(37) Brundle, C. R.; Robin, M. B.; Kuebler, N. A.; Basch, H. *J. Am. Chem. Soc.* **1972**, *94*, 1451.
(38) Parkington, M. J.; Seddon, E. A.; Seddon, K. R.; Stamper, J. G.; Stern, A. M.; Ryan, T. A. *J. Electron Spectrosc. Relat. Phenom.* **1976**, *37*, 395.